



## Research Article

# Effect of Nonmagnetic Doping on Dielectric Properties and Initial Permeability of Ba-Ni Ferrite Nanoparticles by Virtue of Zn<sup>2+</sup> Ions

Sadiq H. Khoreem <sup>1,2,3</sup> and A. H. AL-Hammadi <sup>3</sup>

<sup>1</sup>Physics Department, Faculty of Science, Sa'ada University, Sa'ada, Yemen

<sup>2</sup>Department of Optometry and Vision Science, Faculty of Medical Sciences, Al-Razi University, Sana'a, Yemen

<sup>3</sup>Physics Department, Faculty of Science, Sana'a University, Sana'a, Yemen

Correspondence should be addressed to Sadiq H. Khoreem; khoreems@yahoo.com

Received 30 August 2023; Revised 5 October 2023; Accepted 6 October 2023; Published 16 October 2023

Academic Editor: Hany Abdo

Copyright © 2023 Sadiq H. Khoreem and A. H. AL-Hammadi. This is an open access article distributed under the Creative Commons Attribution License, which permits unrestricted use, distribution, and reproduction in any medium, provided the original work is properly cited.

The effects of composition, temperature, and frequency-dependent dielectric properties of barium-nickel-based ferrites have been investigated. The conventional ceramic technique prepared the compositions BaNi<sub>2-x</sub>Zn<sub>x</sub>Fe<sub>16</sub>O<sub>27</sub> (at x = 0.0, 0.4, 1.2, and 2). The analysis of X-ray diffraction patterns showed that they were single-phase. The average grain size, lattice constant, and density were found to increase as Zn<sup>2+</sup> ion substitution increased. According to the frequency and Zn concentration, the dielectric parameters were properly set. Overall, the dielectric properties of this sample make them a suitable candidate for flexible supercapacitors and are best suited for high-frequency region applications. The initial magnetic permeability of the prepared sample was increasing as the Zn ion contents increases. The produced samples were suitable for application as microwave absorbers, data storage appliances, and magnetic recording mediums.

## 1. Introduction

Nanoparticles have different electrical, optical, microstructural, and magnetic characteristics, which vary compared to the associated bulk state of stability attributes. The small-size impact parameters, surface effect, or quantum influence are to blame for this [1, 2]. Because of their practical significance and technical significance for a variety of applications in industry, electronic devices, magnetic materials, etc., metallic nanoparticles have been extensively and thoroughly studied [3, 4]. According to the structure of their crystals, ferrites can be classified into three groups: spinel ferrite, garnet, and hexagonal ferrites, each of which has a distinct function [5]. However, due to their interesting properties, substituted W-type ferrite possesses promising potential for technological application. These hexagonal ferrites have a ferromagnetic nature at both operating and ambient temperatures. More than 90% of permanent magnets are produced worldwide based on this compound. So, this compound was a deep semiconductor with a ferrimagnetic

structure at room temperature [6–8]. In addition, diamagnetic cations were used to replace the significant spontaneous polarization and multiferric characteristics at room temperature that were recently observed in barium hexaferrite [9]. Various ferrite groups, such as manganese-zinc, nickel-zinc, and magnesium-manganese, are vital for high-tech applications [10–12]. Only nickel-zinc bulk ferrite nanoparticles are promising and suitable for use in high-frequency applications [10, 13, 14]. Eddy currents at high frequencies are a major drawback; that restricts the operation at higher frequencies. This problem can be overcome by increasing the material's electrical resistance and achieving a higher magnetic moment. The electrical resistance can be directly increased by removing the cross-functional and cross-domain walls and converting the material into fine particulate matter [11, 15]. As the grain size increases, grain boundaries form and obstruct the electron passage, reducing eddy current losses [16–19]. The study focuses on investigating the effect of nonmagnetic doping on the dielectric properties and initial permeability

of Ba-Ni ferrite nanoparticles through the introduction of  $Zn^{2+}$  ions. This research is of great pertinence and novelty due to the following reasons:

**Importance of dielectric properties:** dielectric properties play a critical role in various technological applications, including electronics, telecommunications, and energy storage. Understanding the influence of nonmagnetic doping on the dielectric properties of ferrite nanoparticles is crucial for tailoring their electrical characteristics and optimizing their performance in these applications.

**Significance of initial permeability:** The initial permeability is a fundamental magnetic property that determines the response of ferrite materials to magnetic fields. Characterizing the impact of nonmagnetic doping on the initial permeability provides valuable insights into the magnetic behavior and potential applications of the doped ferrite nanoparticles.

**Nonmagnetic doping:** The introduction of  $Zn^{2+}$  ions as a nonmagnetic dopant in Ba-Ni ferrite nanoparticles represents a novel approach to modifying their dielectric and magnetic properties. Investigating the effects of  $Zn^{2+}$  doping on the dielectric properties and initial permeability offers new perspectives on tailoring the performance of ferrite materials for specific applications. In addition, doping BaNi ferrite with Zn ions has attracted significant attention owing to the interesting and enhanced properties of ferrites. Here, we explain the effects of nonmagnetic ion dopants (Zn ions) on barium-nickel nanoferrites. By comprehensively investigating the effect of  $Zn^{2+}$  doping on the dielectric properties and initial permeability of Ba-Ni ferrite nanoparticles, this study aims to contribute to the understanding of the underlying mechanisms and provide valuable insights for the development of advanced ferrite-based materials.

In the present study, the dielectric properties of  $BaNi_{2-x}Zn_xFe_{16}O_{27}$  ( $x = 0, 0.4, 1.2, 2$ ) ferrites were examined as a function of frequency, temperature, and composition, with variation in concentration from  $Zn^{2+}$  ion doping. To produce superior nanoscale ferrites, the right synthesis methods and heating procedures are essential. Additionally, they have had a significant impact on the crystalline composition and dielectric properties of nanoferrites. In this study, we used a ceramic technique to create Zn-substituted BaNi W-HFs with the chemical formula  $BaNi_{2-x}Zn_xFe_{16}O_{27}$  ( $x = 0.0, 0.8, 1.2, 1.6, \text{ and } 2.00$ ). Studies have been done on the impact of  $Zn^{2+}$  concentrations on initial permeability as well as dielectric characteristics.

## 2. Experimental Method

The composition of samples of the  $BaNi_{2-x}Zn_xFe_{16}O_{27}$  W-type hexaferrite (with  $x = 0.0, 0.4, 1.2, \text{ and } 2$ ) has been prepared using the usual ceramics approach, as described previously [20, 21] and depicted in Figure 1. Four tons of pressure was used to press the specimen powder per square centimetre at room temperature to form discs. It gently cooled the discs to ambient temperature by switching the furnace after being sintered at approximately 1250 K to 4 hours. These discs were then polished to create two homogeneous, flat, parallel plate surfaces. Finally, a small layer

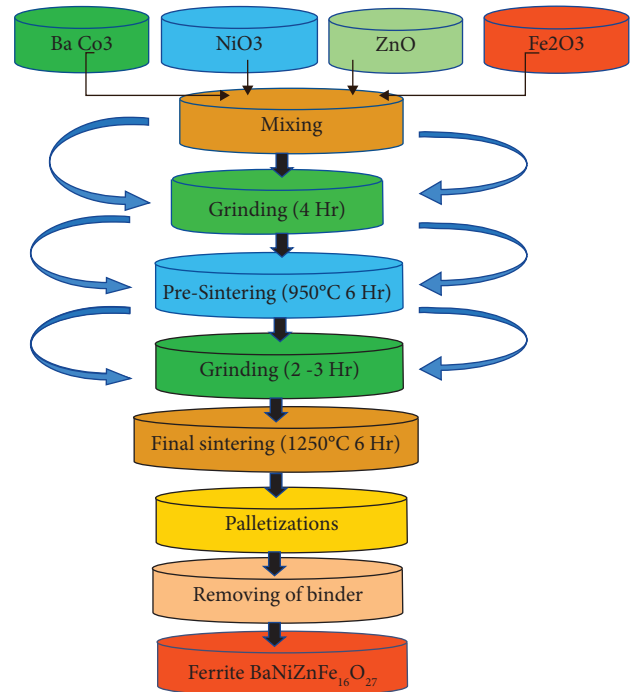


FIGURE 1: Schematic diagram outlining the key steps involved in the sample preparation process.

of silver was applied to the surface to act as a good contact material for measurements of the AC conductivity and dielectric characteristics. We examined the dielectric in vacuum at various temperatures and frequencies using a challenging impedance testing method (Lock-in amplifier, Stanford SR 510 type, USA).

## 3. Results and Discussion

The typical reflections of the  $BaNi_2Fe_{16}O_{27}$ , JCPD card (00-54-0097) with the  $P6_3/mmc$  (194) space group are perfectly equivalent to all the peaks. XRD investigation also confirmed hexagonal W-type single-phase crystalline structures in all samples. Figure 2 demonstrates that all diffraction peaks had a little left shift as a result of Ni being replaced by Zn. The leftward shift of the peaks demonstrated an increase in  $d$ , which demonstrated an increase in the lattice's parameters  $a$  and  $c$ , according to Bragg's formula  $2d\sin = n\lambda$ . Similar to this, utilizing equations and Miller indices (hkl), the pertinent lattice parameters ( $a$  and  $c$ ) were discovered using XRD investigation. When the Zn concentration is increased from 0.0 to 2.0, as seen in Table 1, it increased the lattice parameter. Considering the ionic radii of the substituted ions and the amount of each in the composition, we can describe this behavior. The unit cell volume changes because of the substitution of higher-ionic-radius  $Zn^{2+}$  ions (0.74) for lower-ionic-radius  $Ni^{2+}$  (0.68); the lattice of the crystal is also expanded, which raises the lattice parameters to the same behavior observed in [22–24]. According to the evidence provided by [25] and Vagurd's law, the clear rise in the lattice parameters is constant. According to Vagurd's rule, the ionic radii of the replacing ions determine whether the lattice constant increases or

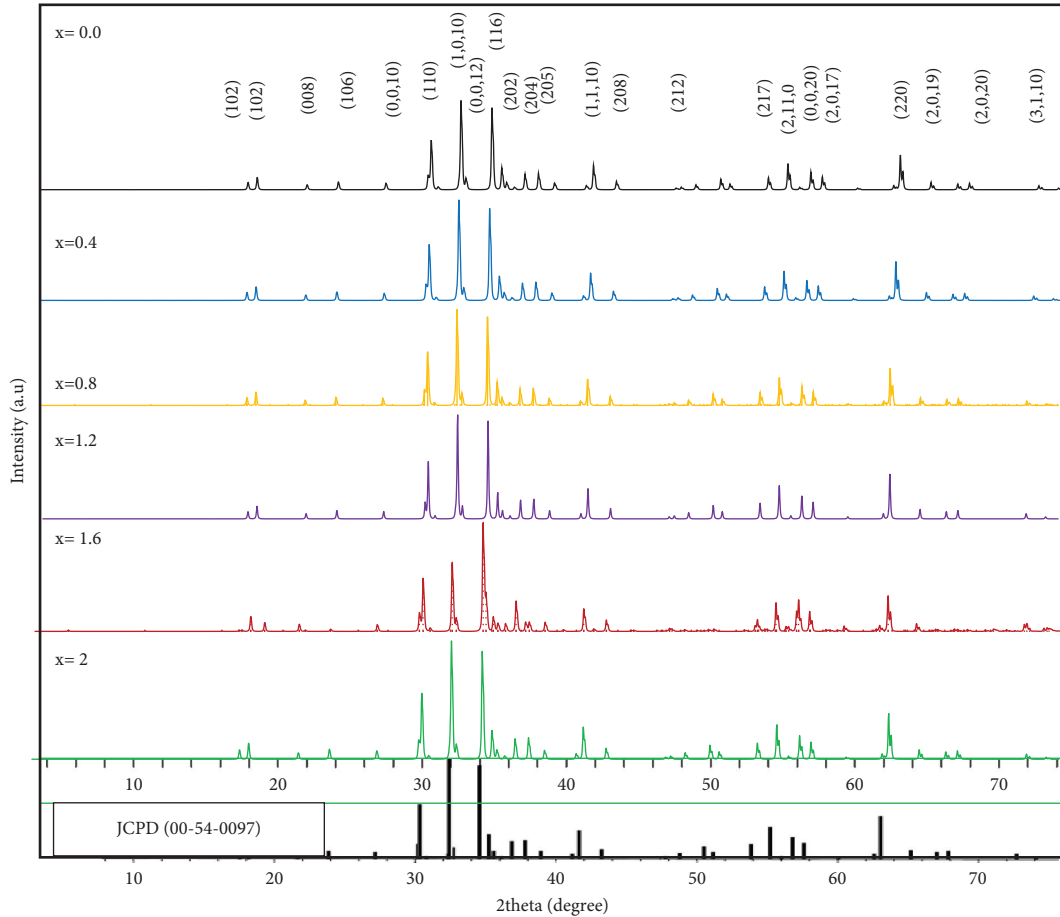


FIGURE 2: XRD pattern of  $\text{BaNi}_{2-x}\text{Zn}_x\text{Fe}_{16}\text{O}_{27}$  ( $x = 0.0, 0.4, 0.8, 1.2, 1.6, \text{ and } 2$ ) with JCPD card (00-54-0097).

TABLE 1: Microstructure constants (grain size, lattice constant, density, and volume).

Zn	$D$ (nm)	$c$ (Å)	$a$ (Å)	$c/a$	$\rho$ (g/cm <sup>3</sup> )	$V$ (Å <sup>3</sup> )
0	35.181	32.734	5.975	5.47849	4.18957	1036.10227
0.4	35.531	32.737	5.976	5.478078	4.27943	1036.5441
0.8	35.814	32.759	5.978	5.47992	4.41655	1037.93507
1.2	36.376	32.784	5.98	5.48227	4.51472	1039.42231
1.6	36.501	32.877	5.981	5.49690	4.55661	1042.71954
2	36.664	32.899	5.997	5.49790	4.62554	1049.00733

decreases linearly. In addition, it was previously shown that the W-type structure can be recognized when its hexagonal lattice parameters  $c/a$  fall between 5.33 and 5.55 which is in agreement with [26, 27]. As shown in Table 1, the value of  $c/a$  in our samples was well within this range, suggesting that the W-type hexagonal structure had formed.

The increase in zinc content in the  $\text{BaNi}_{2-x}\text{Zn}_x\text{Fe}_{16}\text{O}_{27}$  samples can affect the crystalline size and density. When zinc ions ( $\text{Zn}^{2+}$ ) are introduced into the crystal structure as dopants, they can influence the distribution and arrangement of magnetic ions (such as  $\text{Ni}^{2+}$  and  $\text{Fe}^{3+}$ ). With increasing zinc content, several factors come into play. First, as more zinc ions occupy the tetrahedral sites in the crystal lattice, there is a reduction in the number of magnetic ions at these sites. This reduction in magnetic ions at the tetrahedral

sites results in less contact between the tetrahedral and octahedral sites. As a consequence,  $\text{Fe}^{3+}$  ions tend to migrate from the tetrahedral sites to the octahedral sites. The migration of  $\text{Fe}^{3+}$  ions from the tetrahedral to octahedral sites leads to changes in the crystal structure and can affect the crystalline size. It is observed that as the zinc content increases, the crystalline size increases. This increase in crystalline size can be attributed to the rearrangement of ions within the crystal lattice. Furthermore, the increase in the zinc content can also influence the density of the material. As more zinc ions are incorporated into the crystal structure, they occupy space within the lattice, thereby increasing the overall density of the material. For  $\text{BaNi}_{2-x}\text{Zn}_x\text{Fe}_{16}\text{O}_{27}$  samples. Dielectric Properties: The real ( $\epsilon'$ ) and imaginary ( $\epsilon''$ ) components of the dielectric constant were investigated as a function of frequency in the range of 100 kHz to 1 kHz at room temperature (RT) and 438K. The samples exhibited an independent behavior at higher frequencies and an elevated dielectric constant at lower frequencies. The sample with  $x = 0.4$  showed higher values of both the real and imaginary parts of the dielectric constant compared to other samples. Koop's theory was used to explain the high dielectric constant, where the presence of grain boundaries and interfacial dislocations led to Maxwell–Wagner interfacial polarization.

Figures 3(a) and 3(b) show changes in the real ( $\epsilon'$ ) and imaginary ( $\epsilon''$ ) components of the dielectric constant,

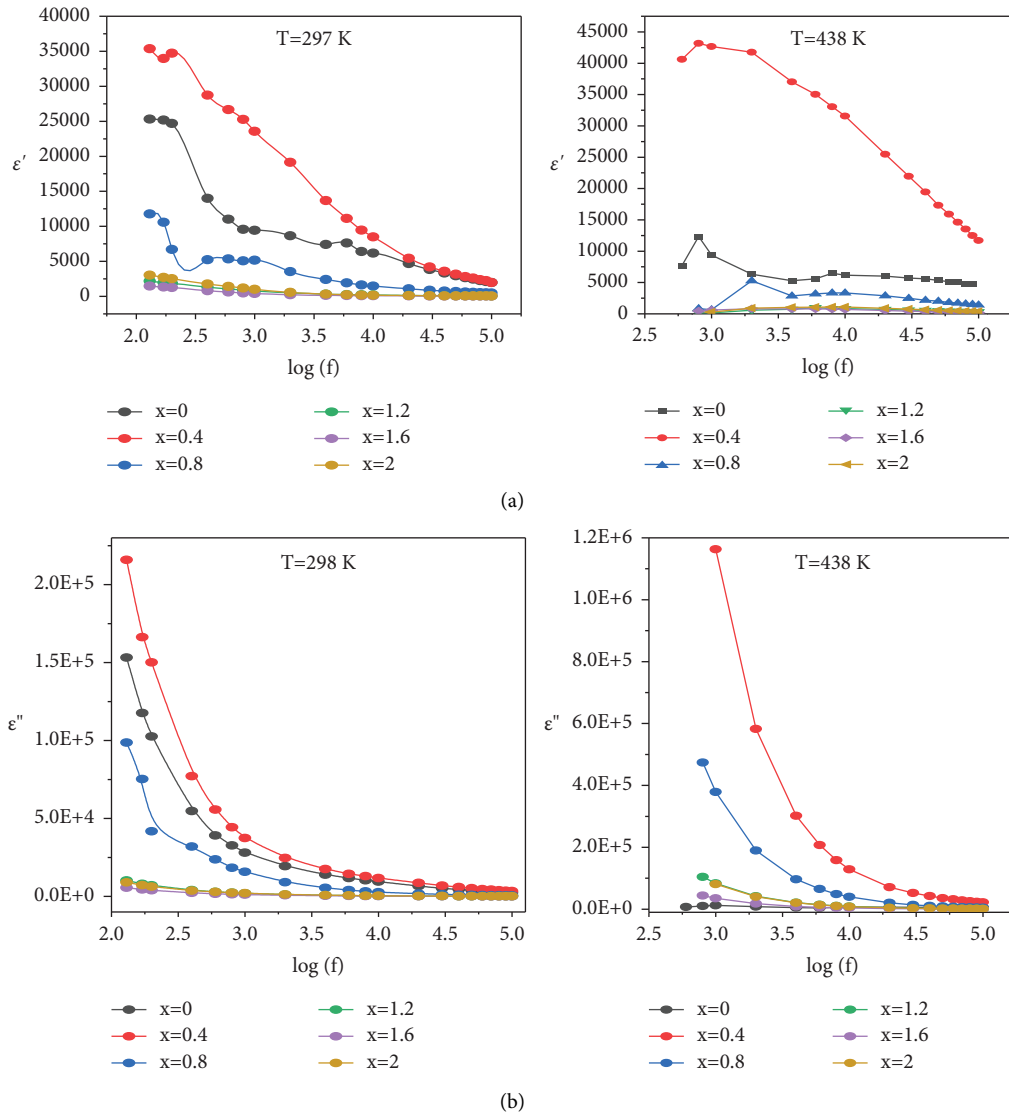


FIGURE 3: Frequency-dependent (a) real dielectric constant and (b) imaginary dielectric constant.

respectively, as a function of frequency in the 100 kHz to 1 kHz range at RT and 438 K. Figure 3(a) shows how the samples, which are representative of all dielectric materials, demonstrated an independent behavior at higher frequencies and an elevated constant for dielectric at lower frequencies. In addition, it can be shown that at  $x = 0.4$ , greater values of the real part and imaginary part  $\epsilon''$  were achieved in comparison to other samples. Koop's theory has been used to explain this kind of high dielectric constant event [28]. According to this concept, the grains and boundaries of grains make up materials that are polycrystalline. The greater and lesser values of the dielectric constant and loss at the highest as well as the lowest frequencies are undoubtedly caused by these two layers present. Based on Koop's theory, grain borders have lower conductivity and higher resistance than crystalline grains, which inhibits charges from travelling and forces them to stay in one place at frequencies that are low. The carriers of charge deposit on the grain boundaries because they cannot move across the boundary.

As a result, Maxwell-Wagner interfacial polarization is produced. The space charge polarization steadily decreases as the input frequency rises. As the energy from the applied field is absorbed, the dipoles become even more active. The result indicates that the grain has higher electrical conductivity and low electrical resistivity. As a result, the dielectric constant value at high frequencies was eventually low. Because of  $\text{Fe}^{2+}$  ion occupancy, within the boundaries of grains, interfacial dislocations, and imperfections, the value of  $\epsilon$  was noticeable at lower frequencies. The interaction between ferrous and ferric ions ( $\text{Fe}^{2+}$  and  $\text{Fe}^{3+}$ ) at the greatest frequencies, however, caused it to diminish. Figure 4(a) illustrates that the electrical dielectric losses were initially significant at low frequencies, decreased as the frequency increased, and then finally proved dependent on the frequency at larger frequencies. When the insulation grain borders opposed electrons, the greatest amount of power was lost [29]. But by offering a significant amount of proof at different frequencies, it gave the electrons enough

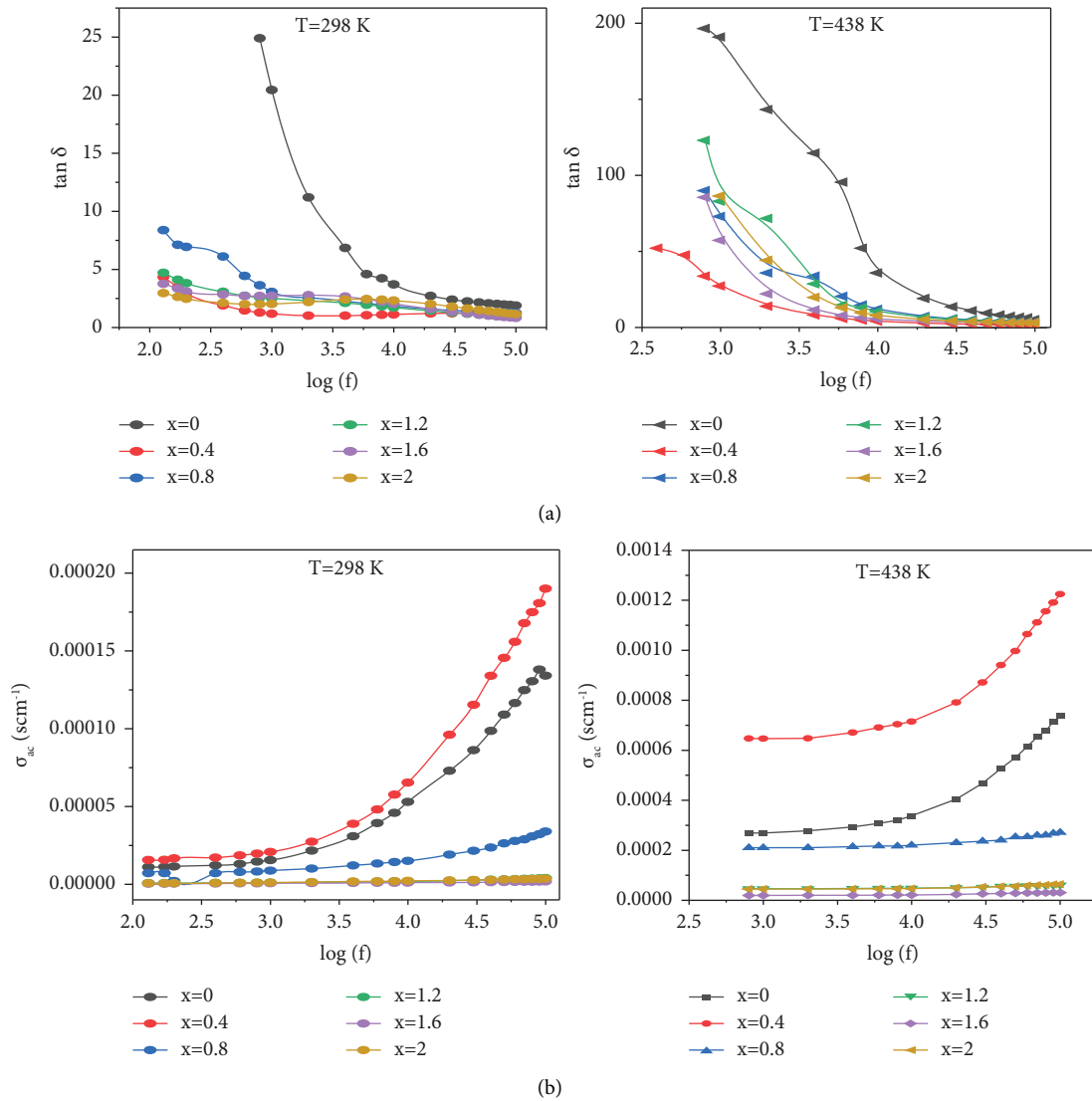


FIGURE 4: (a) Variation of tangent loss with  $\log f$  and (b) variation of AC conductivity with  $\log f$ .

potential to get past the grain’s isolating border. Electrical conductive relaxation, exponential losses, and dielectric oscillation all contributed to the overall dielectric tangent losses.

Figure 4(a) depicts the tangent loss fluctuation as a result of frequency, and all samples initially exhibited minimum tangent loss at lower frequencies. However, when the frequency was increased, the tangent loss rose but then further declined. The samples with  $x = 0.4$  exhibited the lowest tangent loss at intermediate frequencies, but at  $x = 0.0$ , they had the maximum losses.

AC conductivity increases as the applying frequency increases, as shown in Figure 4(b). This phenomenon can be understood using the Maxwell–Wagner bilayer model. This model implies that irritating grain borders separate from the conductive grains. The insulating barriers potentially prevented electron hopping. When the frequency is low, electrons lack the energy to cross through the insulator boundaries of the grains, but as the frequency increases, they

build up enough energy to do so. This way, the ac conductivity rises at higher frequencies. The transmission of electrons at various places causes a conducting behavior in ferrites [30]. Figure 4(b) makes it obvious that the specimen with  $x = 0.4$  has a greater maximum ac conductivity than the other samples. The big polaron hopping behavior in the dc conduction region caused the linear region for samples. As an electrically conducting zone, the higher conductivity mechanism at high frequency contributes to the tiny polaron hopping behavior [31]. Using electric modulus spectroscopy, the voltage response of the samples that were generated has been identified. This technique makes it possible to look into the electrical conductivity, jumping rates, and relaxation processes of electrons. A complex constant of the dielectric has a relationship that is opposite to the electric modulus, which is made up of real ( $M'$ ) and imaginary ( $M''$ ) components. The electric modulus parameter  $M$  serves as a resistive component in hexaferrites. The intricate part demonstrated how the conductivity of the samples was

impacted by the boundaries of the grains and their relaxing behavior [32]. Equations (1) and (2) were used to calculate the values of  $M'$  and  $M''$ , respectively. The subsequent formulae were utilized and used to compute the real ( $M$ ) and imaginary ( $M''$ ):

$$M' = \frac{\epsilon'}{\epsilon'^2 + \epsilon''^2} \quad (1)$$

$$M'' = \frac{\epsilon''}{\epsilon'^2 + \epsilon''^2} \quad (2)$$

Electric modulus: electric modulus spectroscopy was used to analyze the electrical conductivity, hopping rates, and relaxation processes of electrons. The real ( $M'$ ) and imaginary ( $M''$ ) components of the electric modulus were calculated. The magnitude of  $M'$  increased sharply with frequency, indicating rapid hopping and associated charges. The samples exhibited satisfactory agreement between the dielectric constant ( $\epsilon$ ) and  $M''$ . The conduction mechanism was attributed to electron hopping between  $\text{Fe}^{2+}$  and  $\text{Fe}^{3+}$  ions.

Figure 5(a) shows the value of  $M'$  as an indicator of frequency. Inadequate hop charge caused all samples to display the same value at smaller frequencies. As the frequencies rise, the magnitude of  $M'$  rises sharply, showing that hopping begins rapidly and achieves a maximum value because of the elevated associated charges. Figures 3(a) and 5(a) show that  $\epsilon$  and  $M''$  are in satisfactory agreement. None of the conduction occurs at the lower frequencies because real  $\epsilon$  have the lower value and  $M'$  have a high value. At higher frequencies, the higher values of the real part  $M'$  and the smaller values of the real part  $\epsilon$  point to the material's conduct mechanism. In addition, it is believed that the electron jumping between the  $\text{Fe}^{2+}$  ions and  $\text{Fe}^{3+}$  ions at octahedral sites frequently contributes to the conductance of ferrite. The graph with  $x=0.4$  at a typical temperature clearly demonstrates that the resonance peak occurs at higher frequencies. This indicates that the supplied frequency and the hopping frequency of the electron are in phase [33]. Figure 5(b) shows the volatility of  $M''$  frequencies. Every sample showed a noticeable peak, proving that Ba-substituted W-HFs had a relaxing mechanism. The hopping and relaxing processes were present in the samples, as evidenced by the change of peaks in the directions between a high and lower frequency [34]. Doped Ba-Ni ferrite nanoparticles exhibit several properties that make them promising for various industrial applications. Here are some potential industrial applications of doped Ba-Ni ferrite nanoparticles.

Magnetic recording media and microwave devices and telecommunications: Ba-Ni ferrite nanoparticles, when doped with elements such as  $\text{Zn}^{2+}$ , exhibit improved magnetic properties such as high saturation magnetization, coercivity, and remanence. These characteristics make them suitable for use in magnetic recording media, such as hard disk drives (HDDs) and magnetic tapes, where high-density data storage and stable magnetic properties are essential.

3.1. *Permeability.* The initial magnetic permeability of  $\text{BaNi}_{2-x}\text{Zn}_x\text{Fe}_{16}\text{O}_{27}$  was calculated using the following relation [35]:

$$\mu_i = \frac{2\pi L}{\mu_0 N^2 h \ln(a/b)} \quad (3)$$

$b$  represents the internal diameter,  $a$  is its outer diameter,  $L$  represents the inductance,  $N$  is the total number of turns, and  $h$  is the height of the core.

As shown in Figure 6, with increasing zinc concentration, the initial magnetic permeability increased to the maximum value at  $x=2$ . The initial permeability, which is the same as the dielectric constant, is influenced by several factors, including impurity contents, grain structure, compositional type of dopant, crystalline structure, and porosity. The increase in the initial permeability value as Zn concentration increased and vice versa, which, as shown in Figure 6 is due to the grain growth observed with increasing Zn. In addition, it was found that as zinc content increased, the crystalline size and density similarly increased [36], while anisotropy decreased, increasing the initial permeability value [37]. A decrease in initial permeability with temperature is also observed, which is caused by zinc evaporation, which occurs more frequently as the temperature increases, as shown in Figure 7. In W-type hexaferrites, the magnetic ions are distributed between sublattices in a parallel alignment that faces away from the  $c$  axis [38].  $\text{Ni}^{2+}$  ions prefer to occupy octahedral sites,  $\text{Zn}^{2+}$  ions prefer to occupy tetrahedral sites, and  $\text{Fe}^{3+}$  ions are dispersed over both sites. When the nonmagnetic zinc ions on the tetrahedral sites increase,  $\text{Fe}^{3+}$  ions travel from tetrahedral to octahedral sites. Because there is less contact between the tetrahedral and octahedral sites due to the reduction in magnetic ions at the tetrahedral site, the Curie temperature decreases and the initial permeability increases. Because zinc is not magnetic, this behavior occurs naturally, increasing the initial permeability as Zn ions gradually replace Ni ions in the zinc structure. The Curie temperature is the temperature at which a ferromagnetic material undergoes a phase transition and loses its permanent magnetization. Above the Curie temperature, the material transitions into a paramagnetic state, where the magnetic moments become disordered and the material no longer exhibits spontaneous magnetization.

As the temperature increases below the Curie temperature, thermal energy disrupts the alignment of magnetic moments within the material. This disruption leads to a decrease in the net magnetization as the magnetic moments become more randomly oriented. The temperature dependence of magnetization in W-type hexagonal ferrites follows a similar trend, where the magnetization decreases gradually with increasing temperature until it reaches the Curie temperature. Beyond the Curie temperature, the material loses its ferromagnetic properties, and the magnetization drops significantly.

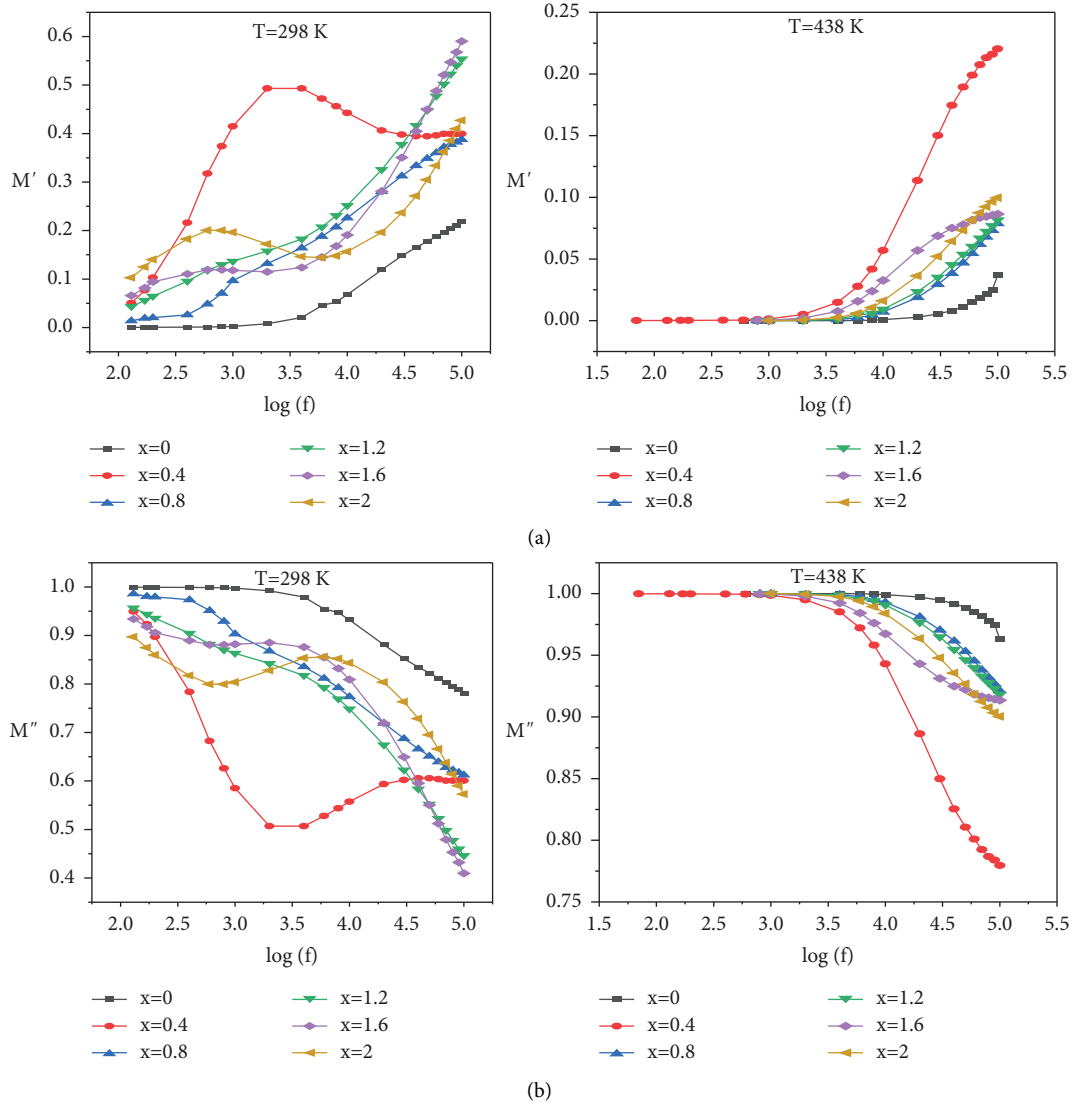


FIGURE 5: (a) Variation of the real part of the electric modulus with  $\log f$  and (b) variation of the imaginary part of the electric modulus with  $\log f$ .

It is worth noting that the specific temperature dependence of magnetization can vary depending on the composition and properties of the ferrite material. However, the general behavior of a gradual decrease in magnetization with increasing temperature until the Curie temperature is a common characteristic observed in W-type hexagonal ferrites and many other ferromagnetic materials. The  $\mu_i-T$  graphs show that when the zinc content rises, the Curie temperature ( $T_c$ ) falls. This is explained because, as the  $Zn^{2+}$  ion level increases, the exchange contract between A and B sites decreases. The distance between the two sites also

increases with an increasing value of “a” with the dopant, which reduces the exchange contact between them. While  $Ni^{2+}$  ions prefer octahedral sites, it dispersed  $Fe^{3+}$  ions throughout both sites, and  $Zn^{2+}$  ions prefer tetrahedral sites.  $Fe^{3+}$  ions move from tetrahedral to octahedral positions as nonmagnetic zinc ions on the tetrahedral sites increase. Because there are fewer magnetic ions  $Ni^{2+}$  at the tetrahedral site, there is less contact between the two sites, which lowers the Curie temperature. According to the published findings [37, 38], the Curie temperature drops as the zinc ion content rises. Zinc is a nonmagnetic substance, and as Zn ions



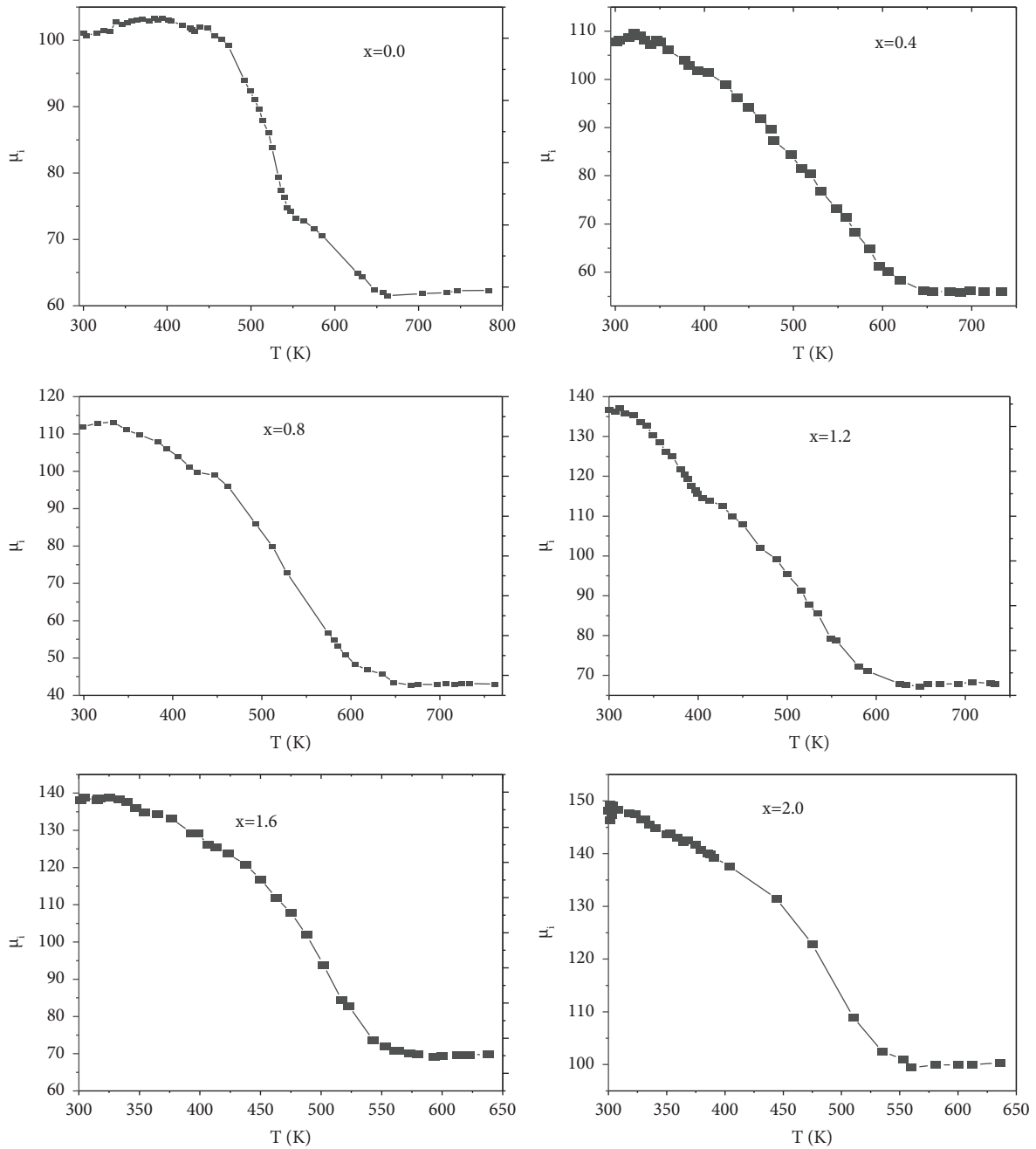


FIGURE 6: Variation of initial permeability with temperature and zinc concentration.

gradually succumb to Ni ions as well, the Curie temperature decreases, causing this event to occur. Overall, the findings imply that the zinc addition significantly affected the material's magnetic and structural properties, increased particle size, decreased porosity, decreased Curie temperature, and

enhanced permeability. This implies that zinc is essential to changing the material's properties. These discoveries may have ramifications for a variety of applications, including the design of magnetic materials with customized properties for certain functions.



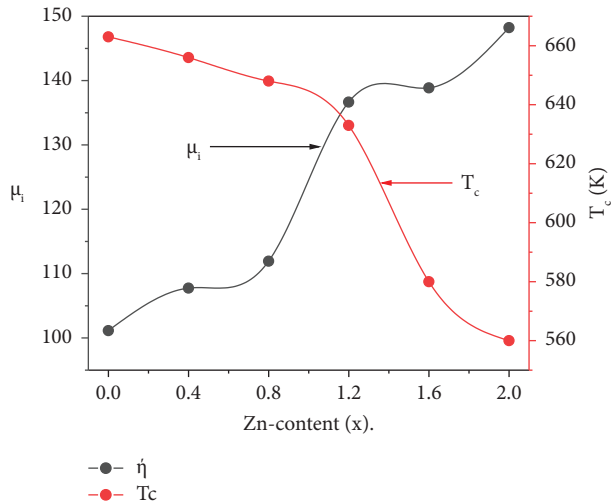


FIGURE 7: Initial permeability and Curie temperature with zinc content.

#### 4. Conclusion

The effects of nonmagnetic ion Zn-doped Ba-Ni based W-type hexaferrite  $\text{BaNi}_{2-x}\text{Zn}_x\text{Fe}_{16}\text{O}_{27}$  ( $x=0.0, 0.4, 0.8, 1.2, 1.6, \text{ and } 2.0$ ) were prepared using the ceramic technique. The electrical conductivity, dielectric constant, and initial magnetic permeability properties were analyzed by CIM. For very efficient photocatalytic microwave absorption devices, this sort of magnetic structure is used. The analysis of X-ray diffraction patterns showed that they were single-phase. The average grain size, lattice constant, and bulk density were found to increase as  $\text{Zn}^{2+}$  ion substitution increased. In order to investigate the samples' dielectric properties, an impedance analyzer has been used. As the frequency increases, both the tangent loss and its dielectric permittivity values decrease. The dielectric results showed that the zinc concentration at composition  $x=0.4$  was sufficient to reduce the dielectric constant and loss tangent at low frequencies, while the dielectric constant had much better results and showed maximum values at  $x=0.4$ . Such material can be dangerously utilized in perpendicular magnetic recording media; however, the dielectric properties of this sample make it a suitable candidate for flexible supercapacitors. The dielectric results demonstrate that a Zn dopant concentration beyond  $\text{Zn}=0.4$  was adequate to reduce both the loss tangent and dielectric constant. This study reveals a wide range of variation in  $\text{Zn}^{2+}$  ion concentration as well as frequency variation, which has not been reported previously. Generally, the decrease in dielectric parameters such as loss tangent and increased dielectric constant resulting from the incorporation of  $\text{Zn}^{+2}$  ions advocate the appropriation of these materials in high-frequency applications such as recording media, sensors, circulators, microwave devices, electronic devices, and phase shifters. The samples' frequency-dependent ac conductivity has grown as their frequencies got higher. The samples' initial permeability to magnetic fields showed an upward trend as Zn concentrations rose and displayed ferromagnetic activity. As  $\text{Zn}^{2+}$  ion replacement increases, the initial magnetic permeability

increases. This might be accounted for by magnetic  $\text{Ni}^{2+}$  ions replacing nonmagnetic  $\text{Zn}^{2+}$  ions. Based on the generated samples may be employed in microwave absorbent and data storage devices based on their magnetic characteristics.

#### Data Availability

The (experimental) data used to support the findings of this study are available from the corresponding author upon request. khoreems@yahoo.com.

#### Conflicts of Interest

The authors declare that they have no conflicts of interest.

#### Acknowledgments

The authors would like to thank Dr. A.M. Abo El Ata and the Physics Department, Faculty of Science, Tanta University, Tanta, Egypt, for his help during the experimental measurements for the present work.

#### References

- [1] M. Hosokawa, *Nanoparticle Technology Handbook*, Elsevier, Amsterdam, Netherlands, 1st edition, 2007.
- [2] J. K. Patel, A. Patel, and D. Bhatia, "Introduction to nanomaterials and nanotechnology," in *Emerging Technologies for Nanoparticle Manufacturing*, J. K. Patel and Y. V. Pathak, Eds., pp. 3–23, Springer International Publishing, Berlin, Germany, 2021.
- [3] Z. A. Gilani, Samiullah, H. M. N. U. H. K. Asghar et al., "Structural, dielectric and electric modulus analysis of praseodymium-substituted  $\text{SrPr}_x\text{Fe}_{12-x}\text{O}_{19}$  nanoparticles synthesized via micro-emulsion," *Applied Physics A*, vol. 129, no. 2, p. 145, 2023.
- [4] Samiullah, H. M. N. U. H. K. Asghar, Z. A. Gilani et al., "Structural, dielectric, impedance and electric modulus properties of praseodymium-substituted  $\text{BaPr}_x\text{Fe}_{12-x}\text{O}_{19}$  nanoparticles synthesized via sol-gel method," *Applied Physics A*, vol. 128, no. 9, p. 762, 2022.
- [5] P. Dhiman, G. Rana, D. Goyal, and A. Goyal, "Basics of ferrites: types and structures," in *Ferrites and Multiferroics: Fundamentals to Applications*, G. K. Bhargava, S. Bhardwaj, M. Singh, and K. M. Batoo, Eds., pp. 1–25, Springer, Singapore, 2021.
- [6] D. A. Vinnik, S. A. Gudkova, V. E. Zhivulin, and E. A. Trofimov, "Ferrite-based solid solutions: structure types, preparation, properties, and potential applications," *Inorganic Materials*, vol. 57, no. 11, pp. 1109–1118, 2021.
- [7] M. Junaid, M. Nadeem, S. A. Abubshait et al., "Impact of Bi-Cr substitution on the structural, spectral, dielectric and magnetic properties of Y-type hexaferrites," *Ceramics International*, vol. 46, no. 16, pp. 25478–25484, 2020.
- [8] A. Charles Prabakar, G. Killivalavan, D. Sivakumar et al., "Exploring structural, morphological, and magnetic properties of zinc nickel ferrites systems nanocomposites," *Bio-interface Research in Applied Chemistry*, vol. 11, pp. 7785–7793, 2020.
- [9] D. A. Vinnik, V. E. Zhivulin, A. Y. Starikov et al., "Influence of titanium substitution on structure, magnetic and electric properties of barium hexaferrites  $\text{BaFe}_{12-x}\text{Ti}_x\text{O}_{19}$ ," *Journal*

- of Magnetism and Magnetic Materials, vol. 498, Article ID 166117, 2020.
- [10] N. S. Mitrović, B. Nedeljković, and N. Obradović, "Magnetic features of MnZn ferrite for electronic applications," in *Proceedings of the Serbian Ceramic Society Conference Advanced Ceramics and Application IX: New Frontiers in Multifunctional Material Science and Processing*, pp. 20-21, Serbia, Belgrade, September, 2021.
  - [11] S. B. Khan, S. Irfan, and S.-L. Lee, "Influence of Zn<sup>2+</sup> doping on Ni-based nanoferrites; (Ni<sub>1-x</sub>Zn<sub>x</sub>Fe<sub>2</sub>O<sub>4</sub>)," *Nanomaterials*, vol. 9, no. 7, p. 1024, 2019.
  - [12] A. K. Pradhan, "Effect of mo substitution on structural, dielectric, electrical and magnetic properties of cobalt-zinc spinel ferrites," Thesis, Vidyasagar University, Midnapore, West Bengal, India, 2021.
  - [13] A. M. Kumar, K. S. Rao, M. C. Varma, and K. H. Rao, "Investigations of surface spin canting in Ni-Zn nanoferrite and its development as magnetic core for microwave applications," *Journal of Magnetism and Magnetic Materials*, vol. 471, pp. 262-266, 2019.
  - [14] P. Thakur, S. Taneja, D. Chahar, B. Ravelo, and A. Thakur, "Recent advances on synthesis, characterization and high frequency applications of Ni-Zn ferrite nanoparticles," *Journal of Magnetism and Magnetic Materials*, vol. 530, Article ID 167925, 2021.
  - [15] E. Pošković, F. Franchini, L. Ferraris, F. Carosio, and M. Actis Grande, "Rapid characterization method for SMC materials for a preliminary selection," *Applied Sciences*, vol. 11, no. 24, Article ID 12133, 2021.
  - [16] M. A. Ahmed, N. Okasha, and S. I. El-Dek, "Preparation and characterization of nanometric Mn ferrite via different methods," *Nanotechnology*, vol. 19, no. 6, Article ID 065603, 2008.
  - [17] P. Andalib and V. G. Harris, "Grain boundary engineering of power inductor cores for MHz applications," *Journal of Alloys and Compounds*, vol. 832, Article ID 153131, 2020.
  - [18] R. Gegevičius, M. Franckevičius, and V. Gulbinas, "The role of grain boundaries in charge carrier dynamics in polycrystalline metal halide perovskites," *European Journal of Inorganic Chemistry*, vol. 2021, no. 35, pp. 3519-3527, 2021.
  - [19] W. Li and L. Fa-Shen, "Structural and magnetic properties of Co<sub>1-x</sub>Zn<sub>x</sub>Fe<sub>2</sub>O<sub>4</sub> nanoparticles," *Chinese Physics B*, vol. 17, no. 5, pp. 1858-1862, 2008.
  - [20] A. H. Al-Hammadi and S. H. Khoreem, "Influence of Zn<sup>2+</sup> doping on dielectric properties of Ba-based nanoferrites," *Biointerface Research in Applied Chemistry*, vol. 13, p. 265, 2022.
  - [21] S. H. Khoreem and A. H. Al-Hammadi, "Synthesis and unveiling the effect of nonmagnetic Zn<sup>2+</sup> ions on enrichment of structural properties of barium-nickel ferrites," *Biointerface Research in Applied Chemistry*, vol. 13, no. 5, 2023.
  - [22] A. A. El-Sayed, "Influence of zinc content on some properties of Ni-Zn ferrites," *Ceramics International*, vol. 28, no. 4, pp. 363-367, 2002.
  - [23] A. Raghavender, N. Biliškov, and Ž. Skoko, "XRD and IR analysis of nanocrystalline Ni-Zn ferrite synthesized by the sol-gel method," *Materials Letters*, vol. 65, no. 4, pp. 677-680, 2011.
  - [24] I. Gul, W. Ahmed, and A. Maqsood, "Electrical and magnetic characterization of nanocrystalline Ni-Zn ferrite synthesis by co-precipitation route," *Journal of Magnetism and Magnetic Materials*, vol. 320, no. 3-4, pp. 270-275, 2008.
  - [25] S. Hasan and B. Azhdar, "Synthesis of nickel-zinc ferrite nanoparticles by the sol-gel auto-combustion method: study of crystal structural, cation distribution, and magnetic properties," *Advances in Condensed Matter Physics*, vol. 2022, Article ID 4603855, 14 pages, 2022.
  - [26] J. E. A. Tang, "Structural, physical, and magnetic analyses of Co-substituted BaFe<sub>2</sub>W-type hexaferrites prepared via the solid-state reaction," *Applied Physics A*, vol. 126, pp. 1-9, 2020.
  - [27] M. N. E. A. Akhtar, S. Javed, M. Ahmad, A. Sulong, and M. A. Khan, "Sol gel derived MnTi doped Co<sub>2</sub>W-type hexagonal ferrites: structural, physical, spectral and magnetic evaluations," *Ceramics International*, vol. 46, no. 6, pp. 7842-7849, 2020.
  - [28] I. M. Musa, Y. Abdu, J. Mohammed, and A. K. Srivastava, "Structural, dielectric and Raman spectroscopy of La<sup>3+</sup>-Ni<sup>2+</sup>-Zn<sup>2+</sup> substituted M-type strontium hexaferrites," *Crystal Research and Technology*, vol. 57, no. 3, 2021.
  - [29] M. Amini and A. Gholizadeh, "Shape control and associated magnetic and dielectric properties of mfe12o19 (M = ba, pb, sr) hexaferrites," *Journal of Physics and Chemistry of Solids*, vol. 147, Article ID 109660, 2020.
  - [30] K. Nadeem, F. Zeb, M. Azeem Abid, M. Mumtaz, and M. Anis ur Rehman, "Effect of amorphous silica matrix on structural, magnetic, and dielectric properties of cobalt ferrite/silica nanocomposites," *Journal of Non-crystalline Solids*, vol. 400, pp. 45-50, 2014.
  - [31] S. F. Mansour, S. Wageh, R. Al-Wafi, and M. A. Abdo, "Enhanced Magnetic, dielectric properties and photocatalytic activity of doped Mg-Zn ferrite nanoparticles by virtue of sm<sup>3+</sup> role," *Journal of Alloys and Compounds*, vol. 856, Article ID 157437, 2021.
  - [32] S. Atiq, M. Majeed, A. Ahmad et al., "Synthesis and investigation of structural, morphological, magnetic, dielectric and impedance spectroscopic characteristics of Ni-Zn ferrite nanoparticles," *Ceramics International*, vol. 43, no. 2, pp. 2486-2494, 2017.
  - [33] M. Shahbaz, I. Sadiq, M. M. Butt et al., "Peculiar magnetic behavior and structural, electrical, dielectric properties of substituted R-type hexagonal ferrites," *Journal of Magnetism and Magnetic Materials*, vol. 499, Article ID 166309, 2020.
  - [34] Z. Hassan, I. Sadiq, R. Hussain et al., "Determination of dual magnetic phases and the study of structural, dielectric, electrical, surface morphological, optical properties of ce<sup>3+</sup> substituted hexagonal ferrites," *Journal of Alloys and Compounds*, vol. 906, Article ID 164324, 2022.
  - [35] J. S. Ghodake, T. J. Shinde, R. P. Patil, S. B. Patil, and S. S. Suryavanshi, "Initial permeability of Zn-Ni-Co ferrite," *Journal of Magnetism and Magnetic Materials*, vol. 378, pp. 436-439, 2015.
  - [36] A. H. Al-Hammadi and S. H. Khoreem, "Investigations on optical and electrical conductivity of Ba/Ni/Zn/fe16o27 Ferrite nanoparticles," *Biointerface Research in Applied Chemistry*, vol. 13, p. 168, 2022.
  - [37] R. V. Mangalaraja, S. T. Lee, S. Ananthakumar, P. Manohar, and C. P. Camurri, "Effect of composition on initial permeability of ni<sub>1-x</sub>zn<sub>x</sub>fe<sub>2</sub>o<sub>4</sub> prepared by Flash Combustion Technique," *Materials Science and Engineering A*, vol. 476, no. 1-2, pp. 234-239, 2008.
  - [38] J.-H. You and S.-I. Yoo, "Improved magnetic properties of zn-substituted Strontium W-type hexaferrites," *Journal of Alloys and Compounds*, vol. 763, pp. 459-465, 2018.